Field-induced light emission from a close-packed Mn-doped ZnS quantum-dot layer in an alternate-current thin-film electroluminescent configuration

Antonio Valerio Longo, Baptiste Notebaert, Alexandre Chevillot, Meriem Gaceur, R. Messina, Alan Durnez, Téo Baptiste, Christophe Dupuis, Ali Madouri, Nicolas Battaglini, et al.

Journal of Applied Physics

Field-induced light emission from a close-packed Mn-doped ZnS quantum-dot layer in an alternate-current thin-film electroluminescent configuration

Cite as: J. Appl. Phys. **131**, 044503 (2022); https://doi.org/10.1063/5.0080328
Submitted: 30 November 2021 • Accepted: 10 January 2022 • Published Online: 28 January 2022

A. V. Longo, B. Notebaert, A. Chevillot, et al.

Journal of Applied Physics ARTICLE scitation.org/journal/jap

Field-induced light emission from a close-packed Mn-doped ZnS quantum-dot layer in an alternate-current thin-film electroluminescent configuration

Cite as: J. Appl. Phys. **131**, 044503 (2022); doi: 10.1063/5.0080328
Submitted: 30 November 2021 · Accepted: 10 January 2022 ·
Published Online: 28 January 2022

A. V. Longo,[1,a)] B. Notebaert,[1,2] A. Chevillot,[1] M. Gaceur,[2] R. Messina,[3] A. Durnez,[4] T. Baptiste,[4] C. Dupuis,[4] A. Madouri,[4] N. Battaglini,[1,a)] and S. Ammar[1]

AFFILIATIONS

[1]Université de Paris, CNRS UMR-7086, ITODYS, 15 rue Jean-Antoine de Baïf, 75205 Paris, France
[2]ACTINOVA SAS, 571 Route de Molières, 82440 Mirabel, France
[3]Université Paris-Saclay, Institut d'Optique Graduate School, CNRS, Laboratoire Charles Fabry, 91127 Palaiseau, France
[4]Université Paris Saclay, CNRS UMR-9001, C2N, 10 Boulevard Thomas Gobert, 91120 Palaiseau, France

[a)]**Authors to whom correspondence should be addressed:** valerio.longo90@gmail.com and nicolas.battaglini@u-paris.fr

ABSTRACT

By exploiting the configuration of an alternate-current thin-film electroluminescent device, we observe the emission of light from a close-packed spin-cast layer of manganese-doped zinc sulfide nanoparticles (NPs), sandwiched between two dielectric layers, induced by the application of an AC voltage. By means of a microwave-assisted polyol synthesis, we are able to obtain high-crystalline surfactant-free NPs, which can be closely packed in the emitting layer, allowing an emission mechanism due to local charge creation and transport, instead of the typical impact-excitation process. This synthesis route allows us to get rid of a bulk semiconductor layer, implying that far less expensive routes for the active layer deposition such as spin coating, inkjet printing, or spray coating can be used. Our work allows us to get a deeper insight into the role played by the NP structure on the charge-transfer mechanism behind light emission and paves the way to a new generation of non-toxic quantum-dot-based displays.

I. INTRODUCTION

Quantum dots[1] form an emerging class of photo- and electroluminescent materials. Their narrow and tunable emission spectrum[2–5] offers the benefits of a broad excitation energy with an environmentally stable and narrow emission, leading to multicolored gap-dependent luminescence. They can be integrated to quantum light electroluminescent diodes[6,7] (QLEDs) as a photo-emissive layer using the blue light from a backlight to emit pure basic colors, improving display brightness and color gamut and reducing light losses and color crosstalk. They can be, for instance, found in recently commercialized LED-backlight liquid crystal displays (LCDs),[8] blue/UV organic LEDs (OLEDs),[9] and micro-LEDs.[10]

They can be also integrated into QLEDs as an electroluminescent layer, stacked within hybrid heterostructures in which holes and electrons, injected from opposite sides through the application of a DC voltage, recombine radiatively in the QD layer.[11–14] This new generation of QD-based LEDs suffers from a major drawback, limiting their large commercialization. Indeed, the materials of the stacked layers should be carefully chosen to optimize the energy-band diagram of the system for efficient electron–hole recombination in the photoactive layer.[15]

Although far less diffused nowadays, a further intriguing way exists to obtain the emission of light from an electroluminescent layer, without any charge-injection process. It consists in sandwiching such a layer between two transparent dielectric layers and applying an alternate electric voltage through two electrodes deposited on the dielectric layers, of which at least one is transparent. This defines the class of ACTFEL (alternate current thin film

electroluminescent) devices. This technology was used in the 1970s to obtain light emission from thick phosphor layers, typically bulk Mn-doped zinc sulfide.[16] The physical mechanism at the origin of the emission of light from these devices is the impact-excitation of the chromophores (the manganese centers), due to free charges moving in the bulk phosphor layer because of the high electric field (EF) induced in it.[17–19] The use of colloidal QDs and the ongoing device miniaturization paved the way to the design of a new generation of devices, the QD-based ACTFELs. The most successful designs were obtained by depositing colloidal heterostructured QDs, typically core–shell II-VI semiconductive nanoparticles (NPs), like CdSe–ZnS, in between submicrometer-sized alumina layers.[20,21] The physical mechanism at the base of the emission of light in these QD-ACTFELs is deeply different from the classical one. Indeed, it is due to a field-induced ionization process caused by a local charge transfer between neighbor QDs. The presence of an EF inside the photoactive region creates a relative shift between the energy levels of NPs at different positions. This allows the generation of electron–hole pairs and their transport within the active layer. The recombination of an electron–hole pair on the same QD is at the origin of the observed light emission,[20] as schematically depicted in Fig. 1.

Beyond these two clear emission mechanisms, a third more complicated configuration was proposed by Wood *et al.* in 2009, the active layer consisting in an arrangement of disordered ZnSe/ZnS:Mn/ZnS core/shell/shell NPs and bulk ZnS layers, light emission stemming from the ZnS:Mn intermediate shell.[22] In the cited work, it was not possible to obtain any emission of light employing only one spin-cast layer of these NPs. To obtain emission of light, it was mandatory to interpose, between several NP layers, films of sputtered bulk ZnS. Although the emission mechanism was not unambiguously clarified, a possible given explanation was that electrons accelerated in the ZnS bulk layer excite Mn in the NP layer again with an impact-based mechanism.

In this work, we report the development of a QD-based ACTFEL device combining the advantages of the two works mentioned above. In fact, we were able to observe light emission from a device implying only one spin-cast NP layer (thus avoiding the more complex multilayer structure of Ref. 22) involving only non-toxic ZnS:Mn NPs (which have proved to have remarkable optical properties and interesting applications[23,24]), instead of the cadmium-based NPs used in Ref. 20. This was made possible thanks to a surfactant-free synthesis, allowing us to obtain a much more compact NP film, favoring charge transport within the active layer. Apart from the more applicative development of the device itself, the work presented here represents an investigation on the possibilities offered by this synthesis route in terms of manipulation of optical activity of non-toxic NPs in a simple structure.

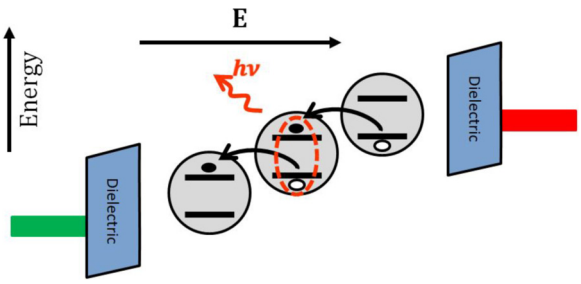

FIG. 1. Simplified schematic representation of the physical mechanism at the origin of light emission in the device presented in Ref. 20. The shift of energy levels of neighbor QD induced by the applied electric field can induce (above a given threshold) the creation of electron–hole pairs (black and white dots in the figure, respectively) and their transport within the QD layer. The recombination of a pair within a single QD leads to light emission.

II. EXPERIMENTS

A. Methods

XRD measurements have been performed on a Panalytical X'pert Pro diffractometer. SEM images have been collected on a FEI Magellan 400 XHR. TEM measurements have been performed on a FEI ThermoFisher TEM/STEM Titan Themis 200 microscope. Impedance measurements have been obtained by the impedance spectrometer Keysight E4980A.

In order to apply the necessary voltage across the device, the sinusoidal signal of a function generator (Gentrad GF266) is amplified in amplitude 20 times by a high-voltage amplifier (Lab System A-303). A resistance of 2.2 kΩ is placed in series with the device in order to limit any current overflow, which could possibly damage it. To measure the AC voltage applied to our devices, two electrodes are connected to the two probes and externally to a digital multimeter.

To measure the intensity–voltage characteristics, a Thorlabs PM130D power meter equipped with a S130C silicon photodiode has been employed. The photodiode has been placed just below the selected contact of the device, in order to collect all the light emitted by the device. This has been possible since the sensitive surface area of the photodiode (diameter of 9.5 mm) is much larger than the emitting contact itself.

Electroluminescence spectra were collected by means of an inverted microscope (Nikon Eclipse Ti-U) allowing us to apply the voltage on top of the device, to collect the focused light from below, and to send it through an optical fiber to high-resolution imaging spectrographs (Oriel MS260i) coupled with a cooled CCD camera (Andor iDus 401).

B. Fabrication and characterization

We now provide the details concerning the stacking of the entire device, of which a schematic view is given in Fig. 2(a) along with an actual picture in Fig. 2(b). The stacking of a typical device starts from a commercially available indium tin oxide (ITO, 80 nm) covered glass substrate. The deposition of the insulating (HfO_2) layers is done by atomic layer deposition, with the deposition temperature of 100 °C and chosen target thickness of 100 nm, using tetrakis (ethyl methylamino) hafnium (TEMAH) as a precursor of metal and H_2O as a precursor of oxygen. Homogeneity and roughness of the HfO_2 layer have been checked by atomic force microscopy (see Fig. 3).

Concerning the NP-based active layer, the synthesis of the involved manganese-doped ZnS (ZnS:Mn) NPs consists in a

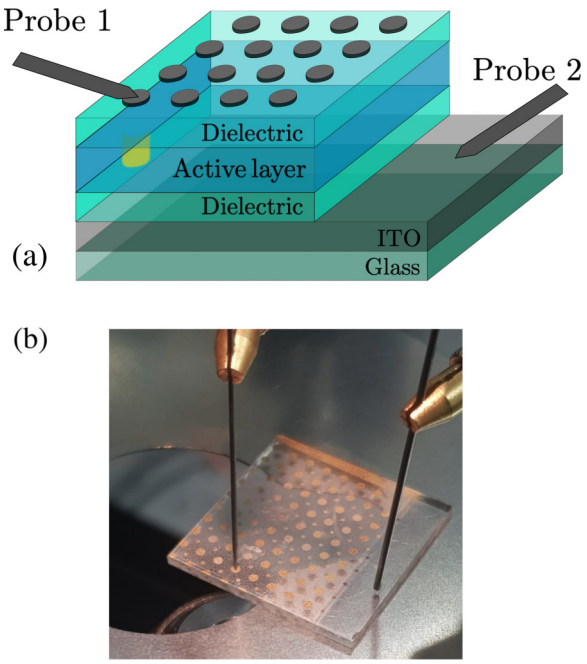

FIG. 2. (a) Sketched section of a QD-ACTEFL device. (b) Actual picture of a full device.

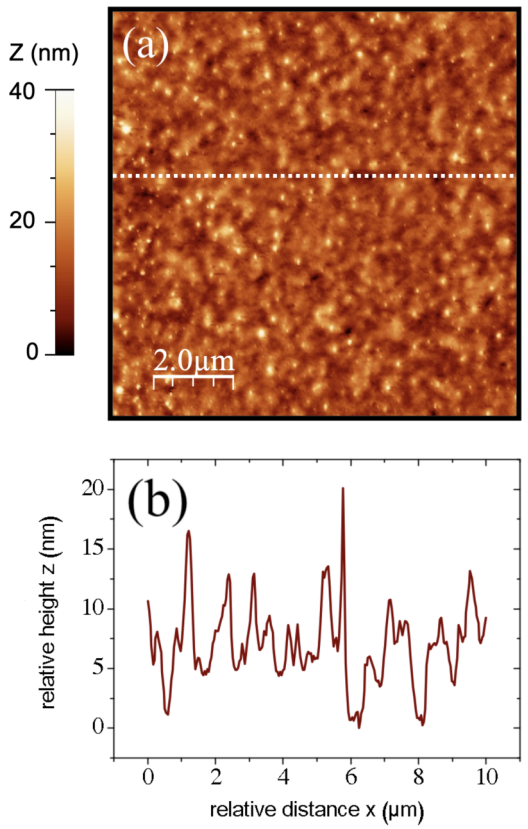

FIG. 3. (a) AFM topography (obtained in the intermittent contact mode) and (b) height profile [corresponding to the dashed line in panel (a)] of a HfO_2 thin film of thickness 100 nm deposited by ALD at 100 °C on ITO. Roughness (RMS value) is 4.5 nm.

microwave-assisted polyol process, using zinc acetate as the zinc source, manganese acetate as the manganese source, and thiocetamide as the sulfur source in a nominal molar metal:sulfur ratio of 1:1.1. The amount of manganese corresponds to a nominal 2% doping. This value allows us to maximize the emission intensity due to Mn centers since it has been shown[25] that higher values have a detrimental effect on this optical activity. Effectively, we have verified that above this value, a decrease of the luminescence is indeed observed. This effect is commonly attributed to a dipolar coupling between Mn ions, which in turn introduces additional non-radiative de-excitation paths.[25] Ethylene glycol is employed as the reaction medium. The as-prepared reaction solution was heated in a multiwave Anton Paar microwave oven for 25 min under a constant radiation power of 220 W. Particles were recovered by centrifugation and then washed by several sessions of dispersion in ethanol and centrifugation. Finally, they were dried at 60 °C overnight.

The obtained NP powder is then dispersed in ethanol and deposited by spin coating on the first dielectric layer. Each spin-coating procedure lasted 30 s, with an angular speed of 2000 rpm attained by an angular acceleration of 4000 rpm/s. A range of concentrations from 20 to 40 mg/ml have been explored (with comparable results), most of the time using the intermediate value of 30 mg/ml. Since the employed NPs are scarcely soluble in ethanol, care was taken of employing the solution for spin coating immediately after the removal from an ultrasonic bath of the flask containing it.

After the deposition of the second dielectric layer, the final stacking step consisted in the deposition of a pattern of electric contacts (Ti/Au or Al, typical thickness of 10/200 and 500 nm, respectively), performed by thermal evaporation through a metallic mechanical mask.

From the XRD measurements performed on NP powder and shown in Fig. 4(a), we can deduce that we obtained NPs with a zinc blende (cubic) structure. In Figs. 4(b) and 4(c), we have a typical global view on how NPs appear under TEM. Moreover, from Fig. 4(c), it is possible to appreciate the excellent crystalline quality of the obtained NPs. Selected area electron diffraction (SAED) [inset in Fig. 4(b)] confirms the cubic structure of the observed NPs, already inferred from XRD measurements. Although NPs tend to aggregate (because of the absence of any surfactant), it is still possible to guess NP contours and thus extract the size of each NP. The inset of Fig. 4(c) shows the observed distribution of NP sizes: the related Gaussian fit is centered at 6.7 nm and has a FWHM of 2.7 nm. Energy-dispersive x-ray (EDX) spectrometry (not shown) allowed us to claim that the ratio between Zn and S is close to 1, and the Mn doping percentage is lower than 2% (around 1.5% as determined by EDX and XPS), in good agreement with x-ray fluorescence measurements.

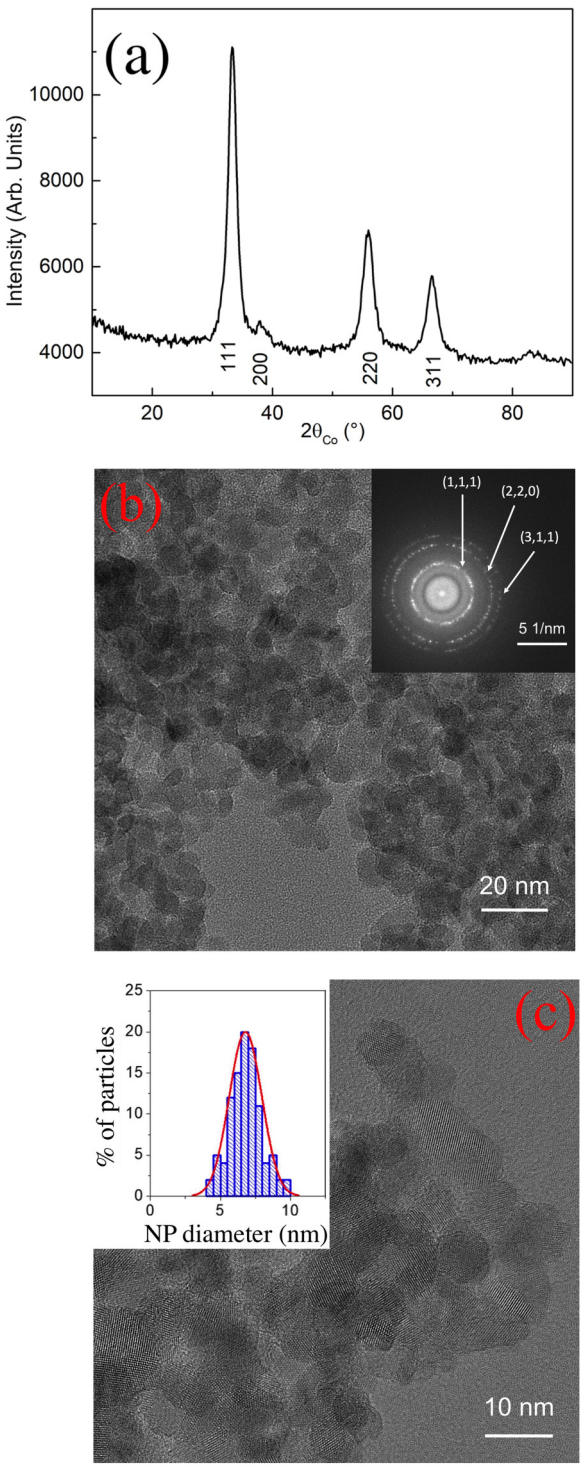

FIG. 4. (a) XRD diffractogram of NP powder. (b) Bright-field TEM images of the NPs. Inset: SAED pattern. (c) Bright-field TEM images of the NPs at a different magnification. Inset: Size distribution of the observed NPs.

Figure 5 shows the absorption and emission spectra of the NPs. In particular, it is possible to observe in Fig. 5(a) an absorption spectrum (red curve) presenting a monotonic increase when going toward lower wavelengths, although a slight shoulder of this ramp can be seen around 330 nm, which can be ascribed to band-to-band transitions. The emission shown in Fig. 5(a) (black curve) is due to excitonic recombination and peaks in the UV region, around 330 nm. Figure 5(b) shows instead the emission due to Mn doping, associated with the $^4T_1$–$^6A_1$ transition and peaking as expected around 590 nm.

We finally address the features of the performed depositions, exploiting a dedicated sample implying only the first dielectric layer and the active layer. The results of its scanning electron microscopy analysis are shown in Fig. 6. The active layer is easily identifiable because of the net contrast with respect to the layer below, and the spin-coated films present a very compact structure.

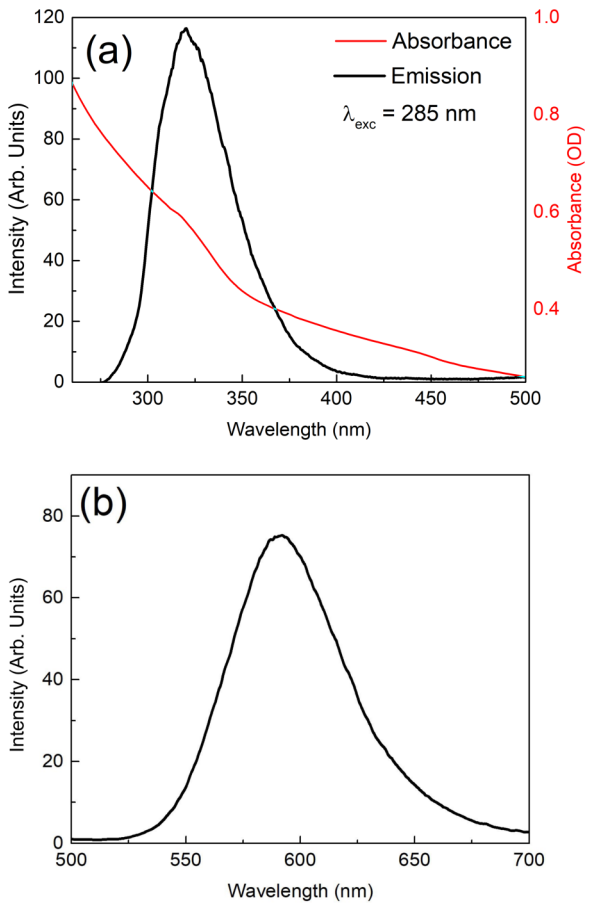

FIG. 5. (a) UV–Visible absorption (red line) and emission (black) spectra. The peak around 320 nm is associated with excitonic recombination taking place in ZnS crystal host. (b) Emission spectrum in the 500–700 nm wavelength range, where the main peak around 590 nm stems from the $^4T_1$-$^6A_1$ transition associated with Mn centers. For panel (b), the excitation wavelength is 300 nm.

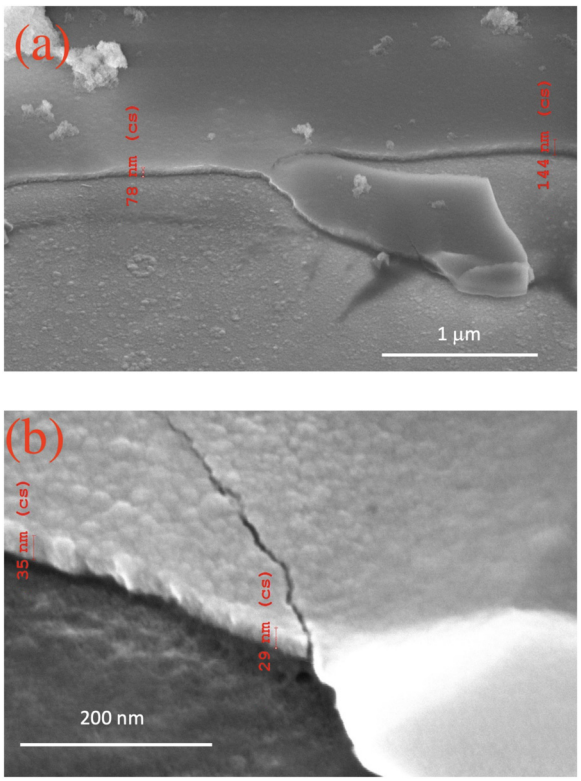

FIG. 6. SEM images at (a) lower and (b) higher magnification of specifically prepared samples involving only the ITO-covered glass substrate, a first dielectric layer, and the active NP layer.

These images allow us to graphically estimate the local thickness of the active layer, for which we observe a high variability, ranging from tens of nm to around 140 nm.

III. OBSERVATION OF LIGHT EMISSION

To study the intensity of the emitted light as a function of the applied voltage, a power meter equipped with a silicon photodiode has been employed (see Sec. II A). On several devices, we have recorded the intensity of emitted light by varying the applied voltage and working at a frequency of 30 kHz. Figure 7(a) shows several light intensity/voltage characteristics. We clearly confirm the anticipated threshold behavior and observe an increase of the intensity above threshold. All the curves share the same qualitative behavior, with a threshold voltage around 50 V. The values of the threshold voltage for the collected data sets are {48, 68, 57, 55, 75, 54, 54, 54} V: we observe that a value around 54 V is often encountered, with three exceptions having both lower and higher values. The value $54\sqrt{2}$ V (54 V being an RMS value) allows us to estimate the threshold electric field inside the active layer. Assuming a uniform permittivity within the device, and taking 90 nm as an average thickness of the active layer, one obtains 2.6 MV/cm. This value is close to the one observed in Ref. 20.

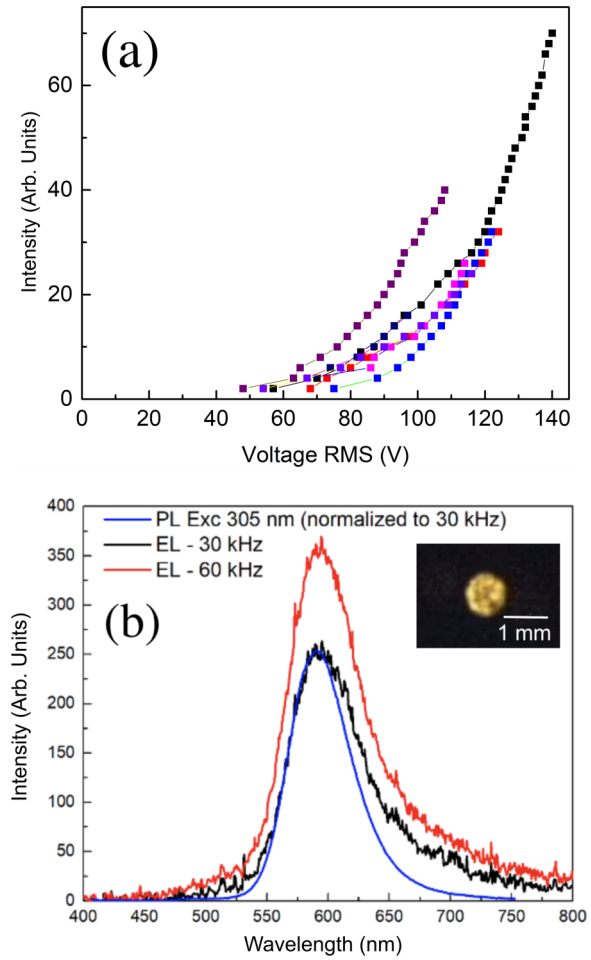

FIG. 7. (a) Intensity–voltage characteristics of the device. (b) Electroluminescence spectra collected under an applied AC voltage of 70 V (both black and red lines), fixing the frequency at 30 and 60 kHz (black and red lines, respectively), compared to the photoluminescence one measured on the ZnS:Mn QD layer alone (blue line). In the inset, a picture from the device during emission (75 V RMS, 30 kHz).

We now address the spectral properties of the light emitted from our device. In order to collect EL spectra, an inversed microscope and a spectrophotometer coupled with an optical fiber have been employed (see Sec. II A). In Fig. 7(b), we show EL spectra collected at an applied alternate voltage above threshold (around 70 V), with a frequency of 30 or 60 kHz, along with the PL spectrum collected from the NP layer alone (excitation wavelength of 300 nm). The ratio between the intensity collected at the two frequencies is in excellent agreement with square-root dependence of the intensity on the frequency.[21] A direct comparison between EL and the PL spectra clearly shows that the observed luminescence corresponds to the emission coming from the transition taking place in Mn ions.

IV. PHYSICAL DISCUSSION ON THE EMISSION MECHANISM

As discussed above, in conventional ACTFEL devices, the electroemissive behavior is explained by an impact-excitation mechanism. On the other hand, the device described by Wood *et al.* in 2011,[20] although implying the same arrangement of insulating and emitting layers, works under a totally different field-induced emission mechanism based on local charge creation and transfer between neighbor QDs.

To understand whether an impact-excitation mechanism could be at the origin of the observed light emission, we exploited previous Monte Carlo simulations studying the electron dynamics in bulk Mn-doped ZnS.[26–29] Impact-excitation phenomena are treated as a specific class of scattering events taken into account in these simulations.

We could first assume that each NP behaves as a small portion of a bulk material and could host electron acceleration. This description neglects the fact that the average size of each NP (around 7 nm) is not much larger than the exciton Bohr radius of ZnS (2.5 nm), implying that a semi-classical treatment of electron dynamics could not be rigorous in the first place, the NP possibly being in a transition regime toward an atomic-like system. Ignoring this limitation, we considered the time evolution of the electron drift velocity (along the electric-field direction), calculated for different applied fields in Ref. 29. We have numerically extracted the time needed for an electron to travel across the entire NP, obtaining 15 and 24 fs for $E = 1$ and $E = 2$ MV/cm, respectively. By inspecting the average electron energy as a function of time with or without taking into account impact-excitations (see Ref. 29), we concluded that impact-excitation plays a role starting from around 200 fs. As a consequence, within the time needed for an electron to travel across the NP, impact-excitation cannot be effective to induce EL. This is confirmed by Ref. 28, studying in detail the transient dynamics of electrons under the action of an external electric field, clearly stating that the reaching of a steady-state regime is mandatory in order to obtain EL from impact excitation. Again, this condition is clearly not satisfied in a 7 nm NP.

Another scenario could still be consistent with an impact-excitation mechanism, namely, the entire disordered NP layer behaving as a bulk. In this case, the possibility that electrons could hop from a NP to another one has to be introduced. Of course, this phenomenon is fundamentally different from all the scattering events mentioned above, since the electron would move from the lattice of a given NP to another one. As already discussed in Ref. 20, the efficiency of such an interaction would produce a significant reduction of the electron kinetic energy, implying that the electron would start again its motion along the active layer from near-zero kinetic energy. This discussion allows us to fully exclude an impact-excitation mechanism.

We are thus left with the hypothesis of the mechanism already described in Ref. 20, i.e., local creation and transport of charges along the active layer, followed by radiative recombination within a given QD. Our interpretation is that this mechanism works in our devices and not in the ones realized in Ref. 22 because our synthesis procedure allowed us to obtain an active layer with a significantly higher packing of NP. This is consistent with the fact that the NPs in Ref. 22 were synthesized using surfactants and have a much more elaborated heterostructure. In order to have an indication of our high NP density, we have followed the approach employed in Ref. 21, based on the Maxwell–Garnett effective-medium approach,[30] describing a medium composed of two different materials (host and inclusion) as a uniform medium characterized by an effective permittivity ε_{eff}. This approach is strictly valid only in the limit of low filling fraction f, i.e., the ratio of volume occupied by the inclusions with respect to the total volume. As a consequence, the use of this framework to prove a high filling fraction f must be taken only as the indication of a trend as a function of some external parameters and not as a tool to extract a rigorous value of the NP density.

If the host medium (resp. inclusions) has permittivity ε_h (resp. ε_i), the Maxwell–Garnett theory gives the following expression of the effective permittivity:

$$\varepsilon_{\text{eff}} = \varepsilon_h \frac{\varepsilon_h + \frac{1+2f}{3}(\varepsilon_i - \varepsilon_h)}{\varepsilon_h + \frac{1-f}{3}(\varepsilon_i - \varepsilon_h)}. \tag{1}$$

By impedance-spectroscopy measurements, we obtained the capacitance C of our full device, along with the permittivity of the dielectric layers $\varepsilon_{\text{diel}} \simeq 10.7$. These values can be employed to estimate the effective dielectric permittivity ε_{eff} and the filling fraction f. The former reads

$$\varepsilon_{\text{eff}} = \frac{\varepsilon_{\text{diel}} d_{\text{al}} C}{\varepsilon_0 \varepsilon_{\text{diel}} S - 2 d_{\text{diel}} C}, \tag{2}$$

with S being the surface of the device. Moreover, from Eq. (1), by assuming vacuum as the host material ($\varepsilon_h = 1$) and noting with ε_{ZnS} the permittivity of ZnS inclusions, we obtain the filling fraction

$$f = \frac{(\varepsilon_{\text{ZnS}} + 2)(\varepsilon_{\text{eff}} - 1)}{(\varepsilon_{\text{ZnS}} - 1)(\varepsilon_{\text{eff}} + 2)}. \tag{3}$$

The measured capacity of the entire device is 190 pF, and we take $d_{\text{diel}} = 100$ nm as a fixed value. On the contrary, based on SEM observations (see Fig. 6), we keep the thickness of the active layer d_{al} as a variable parameter. Using these parameters, Eq. (2) allows us to obtain an estimate of the effective permittivity of the active layer of 7.6, making the assumption of uniform permittivity within the device made above reasonable.

The last parameter needed to determine the filling fraction f as a function of d_{al} is the permittivity of ZnS inclusions. It is known that in the case of particles of nm size, the permittivty can differ significantly from the one of the bulk (around 8.9 for ZnS). This has been observed experimentally[31–34] and recently discussed theoretically for different kinds of quantum dots.[35] In the case of ZnS, measurements have shown that at the frequency of interest for our work (around 30 kHz), the permittivity for NP having the size of some nm is around 100[31,33,34] or above.[32] Equation (3) clearly shows that, for these values of ε_{ZnS}, f becomes independent of ε_{ZnS} and equal to $(\varepsilon_{\text{eff}} - 1)/(\varepsilon_{\text{eff}} + 2)$.

The obtained filling fraction f as a function of d_{al} is shown in Fig. 8(a). We observe that in a wide range of observed values of the active-layer thickness, we obtain a high value of the filling fraction

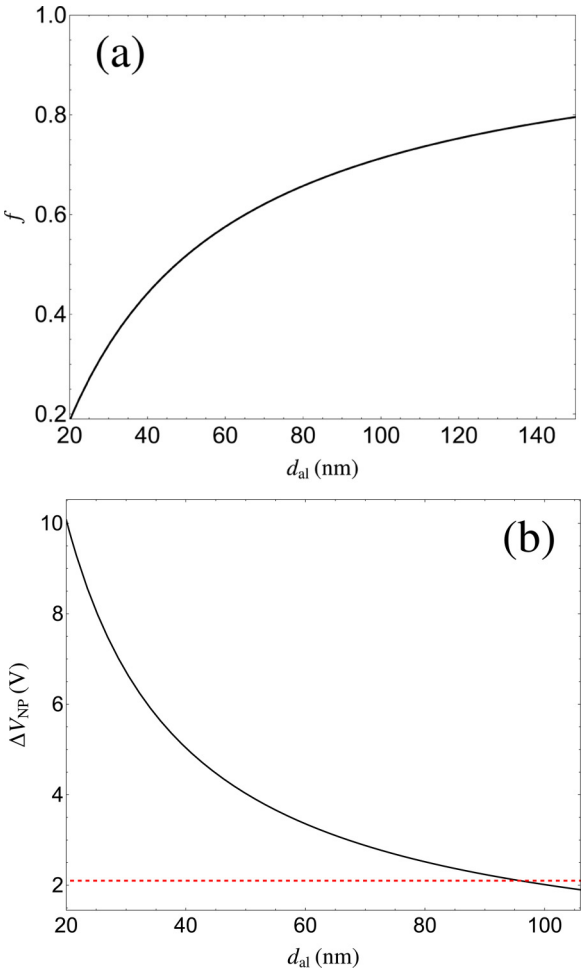

FIG. 8. (a) NP filling fraction f and (b) potential difference per NP as a function of the thickness d_{al} of the active layer obtained by means of the Maxwell–Garnett theory. The red dashed line in (b) corresponds to the energy of emitted light.

growing as a function of d_{al}, reaching and going beyond the value $f = 74\%$, corresponding to the maximum allowed in a close-packing configuration involving spherical inclusions. Because of these high values of f, we stress again that an effective-medium approach is not supposed to provide in our scenario a reliable quantitative estimate of the filling fraction. Nevertheless, these values could be taken as an indication of the high NP density in our film, made possible by our synthesis technique and allowing for an efficient charge transfer between neighboring NP.

The effective permittivity also allows us to estimate the value of the potential energy drop per NP as a function of the thickness d_{al} and in this case also of the externally applied voltage ΔV. This reads

$$\Delta V_{NP} = \frac{\varepsilon_{diel}\Delta V d}{2\varepsilon_{al}d_{diel} + \varepsilon_{diel}d_{al}}, \quad (4)$$

with d being the diameter of each NP. Taking $d = 6.7$ nm for the NP diameter and the threshold value $\Delta V = 55\sqrt{2}$ V for the applied voltage, we obtain the curve shown in Fig. 8(b), along with the value 2.1 eV corresponding to the energy of emitted light. This represents then the energy threshold above which the mechanism described above can take place. We observe that for a wide range of observed thicknesses, ΔV_{NP} is above 2.1 eV. Notwithstanding the simplicity and limitations of this model, this corroborates our interpretation of the physical mechanism (based on local charge creation and transport) at the origin of light emission.

V. CONCLUSIONS

We have investigated the electroluminescence mechanism of ZnS:Mn NPs under an ionization field produced in a QD-based ACTFEL light-emitting device. On this device, we have observed a threshold mechanism for the intensity of emitted light as a function of applied voltage, the voltage threshold value being around 50 V RMS. Moreover, a comparison of electroluminescence and photoluminescence spectra has allowed us to clearly ascribe the emission from the device to the Mn centers in Mn-doped ZnS NPs embedded in the active layer. We have then focused on the study of the physical origin of light emission, and we have been able to rule out an impact-excitation mechanism. On the contrary, light emission in our device stems from a field-induced charge creation and transport process, obtained for Mn-doped ZnS NPs in a simple dielectric–active layer–dielectric configuration, as a result of a compact NP film coming from our synthesis route. Our work constitutes a step forward in the development of more compact, industrially feasible, and eco-friendly light-emitting devices.

ACKNOWLEDGMENTS

This work was supported by the French ANR (Agence Nationale de la Recherche) and CGI (Commissariat à l'Investissement d'Avenir) through Labex SEAM grant (Nos. ANR-11-LBX-086 and ANR-11-IDEX-0502). The presented research was also supported by the French National Research and Education Network (RENATECH). The authors acknowledge G. Patriarche for the fruitful support for TEM measurements.

AUTHOR DECLARATIONS

Conflict of Interest

The authors have no conflicts to disclose.

DATA AVAILABILITY

The data that support the findings of this study are available from the corresponding authors upon reasonable request.

REFERENCES

[1]A. Ekimov, A. Efros, and A. Onushchenko, Solid State Commun. **56**, 921 (1985).
[2]L. Brus, J. Phys. Chem. **90**, 2555 (1986).
[3]D. Bera, L. Qian, T.-K. Tseng, and P. H. Holloway, Materials **3**, 2260 (2010).
[4]P. Alivisatos, Nat. Biotechnol. **22**, 47 (2004).
[5]X. Gao, Y. Cui, R. M. Levenson, L. W. K. Chung, and S. Nie, Nat. Biotechnol. **22**, 969 (2004).

[6]Y. Shirasaki, G. J. Supran, M. G. Bawendi, and V. Bulović, Nat. Photonics **7**, 13 (2013).
[7]Z. Yang, M. Gao, W. Wu, X. Yang, X. W. Sun, J. Zhang, H.-C. Wang, R.-S. Liu, C.-Y. Han, H. Yang, and W. Li, Mater. Today **24**, 69 (2019).
[8]C.-F. Lai, Y.-C. Tien, H.-C. Tong, C.-Z. Zhong, and Y.-C. Lee, RSC Adv. **8**, 35966 (2018).
[9]N. Thejokalyani and S. J. Dhoble, Renewable Sustainable Energy Rev. **32**, 448 (2014).
[10]Z. Liu, C.-H. Lin, B.-R. Hyun, C.-W. Sher, Z. Lv, B. Luo, F. Jiang, T. Wu, C.-H. Ho, H.-C. Kuo, and J.-H. He, Light Sci. Appl. **9**, 83 (2020).
[11]Y. Yang, Y. Zheng, W. Cao, A. Titov, J. Hyvonen, J. R. Manders, J. Xue, P. H. Holloway, and L. Qian, Nat. Photonics **9**, 1 (2015).
[12]X. Dai, Z. Zhang, Y. Jin, Y. Niu, H. Cao, X. Liang, L. Chen, J. Wang, and X. Peng, Nature **515**, 96 (2014).
[13]H. Zhang, X. Sun, and S. Chen, Adv. Funct. Mater. **27**, 1700610 (2017).
[14]H. Zhang, S. Chen, and X. W. Sun, ACS Nano **12**, 697 (2018).
[15]V. Wood, M. J. Panzer, J. E. Halpert, J.-M. Caruge, M. G. Bawendi, and V. Bulović, ACS Nano **3**, 3581 (2009).
[16]T. Inoguchi, M. Takeda, Y. Kakahara, Y. Nakata, and M. Yoshida, SID 74 Digest **5**, 84 (1974).
[17]J. F. Wager and P. D. Keir, Annu. Rev. Mater. Sci. **27**, 223 (1997).
[18]A. N. Krasnov and P. G. Hofstra, Prog. Cryst. Growth. Charact. Mater. **42**, 65 (2001).
[19]A. Kitai, *Luminescent Materials and Applications*, Wiley Series in Materials for Electronic and Optoelectronic Applications (John Wiley, Hoboken, NJ, 2008).
[20]V. Wood, M. J. Panzer, D. Bozyigit, Y. Shirasaki, I. Rousseau, S. Geyer, M. G. Bawendi, and V. Bulović, Nano Lett. **11**, 2927 (2011).
[21]D. Bozyigit, V. Wood, Y. Shirasaki, and V. Bulović, J. Appl. Phys. **111**, 113701 (2012).
[22]V. Wood, J. E. Halpert, M. J. Panzer, M. G. Bawendi, and V. Bulović, Nano Lett. **9**, 2367 (2009).
[23]B. B. Srivastava, S. Jana, N. S. Karan, S. Paria, N. R. Jana, D. D. Sarma, and N. Pradhan, J. Phys. Chem. Lett. **1**, 1454 (2010).
[24]M. Geszke-Moritz, H. Piotrowska, M. Murias, L. Balan, M. Moritz, J. Lulekb, and R. Schneider, J. Mater. Chem. B **1**, 698 (2013).
[25]A. Nag, S. Chakraborty, and D. D. Sarma, J. Am. Chem. Soc. **130**, 10605 (2008).
[26]K. Bhattacharyya, S. M. Goodnick, and J. F. Wager, J. Appl. Phys. **73**, 3390 (1993).
[27]J. Fogarty, W. Kong, and R. Solanki, Solid-State Electron. **38**, 653 (1995).
[28]Z. Hui, W. Yongsheng, X. Zheng, and X. Xurong, J. Phys.: Condens. Matter **11**, 2145 (1999).
[29]M. Dur, S. M. Goodnick, S. S. Pennathur, J. F. Wager, M. Reigrotzki, and R. Redmer, J. Appl. Phys. **83**, 3176 (1998).
[30]V. A. Markel, J. Opt. Soc. Am. A **33**, 1244 (2016).
[31]N. Soltani, A. Dehzangi, A. Kharazmi, E. Saion, W. Mahmood Mat Yunus, B. Yeop Majlis, M. Reza Zare, E. Gharibshahi, and N. Khalilzadeh, Chalcogenide Lett. **11**, 79 (2014).
[32]S. Ganguly, K. Halder, N. A. Haque, S. Das, and S. G. Dastidar, Am. J. Res. Commun. **3**, 68 (2015).
[33]S. Suresh, Int. J. Phys. Sci. **8**, 1121 (2013).
[34]P. K. Ghosh, S. Jana, S. Nandy, and K. K. Chattopadhyay, Mater. Res. Bull. **42**, 505 (2007).
[35]S. Zare and S. Edalatapour, J. Appl. Phys. **130**, 015108 (2021).